HHS Public Access

Author manuscript

*Biochemistry*. Author manuscript; available in PMC 2020 March 24.

Published in final edited form as:

*Biochemistry*. 2018 December 11; 57(49): 6787–6796. doi:10.1021/acs.biochem.8b00907.

# Hinge-linker elements in the AAA+ protein unfoldase ClpX mediate intersubunit communication, assembly, and mechanical activity

**Tristan A. Bell**[1], **Tania A. Baker**[1,2], **Robert T. Sauer**[1,*]

[1]Department of Biology, Massachusetts Institute of Technology, Cambridge, MA 02139

[2]Howard Hughes Medical Institute, Massachusetts Institute of Technology, Cambridge, MA 02139

## Abstract

The ClpXP protease plays important roles in protein homeostasis and quality control. ClpX is a ring-shaped AAA+ homohexamer that unfolds target proteins and translocates them into the ClpP peptidase for degradation. AAA+ modules in each ClpX subunit — consisting of a large AAA+ domain, a short hinge-linker, and a small AAA+ domain — mediate the mechanical activities of the ring hexamer. Here, we investigate the roles of these hinge-linkers in ClpX function. Deleting one hinge-linker in a single-chain ClpX pseudohexamer dramatically decreases unfolding and degradation activity, in part by compromising formation of closed rings, protein-substrate binding, and ClpP binding. Covalently reclosing the broken hinge-linker interface rescues activity. Deleting one hinge-linker from a single-chain dimer or trimer prevents assembly of stable hexamers. Mutationally disrupting a hinge-linker preserves closed ring assembly but reduces ATP-hydrolysis cooperativity and degradation activity. These results indicate that hinge-linker length and flexibility are optimized for efficient substrate unfolding and support a model in which the hinge-linkers of ClpX facilitate efficient degradation both by maintaining proper ring geometry and facilitating subunit-subunit communication. This model informs our understanding of ClpX as well as the larger AAA+ family of motor proteins, which play diverse roles in converting chemical into mechanical energy in all cells.

## Graphical Abstract



[*]**Correspondence:** bobsauer@mit.edu.

Author contributions

T.A. Bell performed experiments. T.A. Bell, T.A. Baker, and R.T.S. designed experiments and analyzed data. T.A. Bell and R.T.S. wrote the manuscript. All authors approved the final version of the manuscript. The authors declare no competing financial interests.

UniProt Accession IDs

ClpX: P0A6H1

ClpP: P0A6G7

Arc: P03050

GFP: P42212

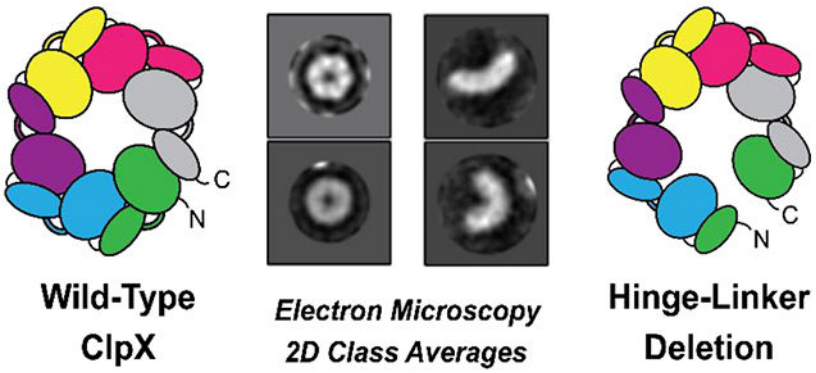


**Keywords**

ClpXP; AAA+ enzymes; ATP-dependent protein unfolding; protein degradation

## Introduction

All organisms require the ability to convert chemical energy into mechanical work. Members of the AAA+ protein family (ATPases associated with various cellular activities) use ATP hydrolysis to power many cellular mechanical processes, including protein unfolding and disaggregation[1]. Typical family members assemble into ring- or spiral-shaped structures, often hexamers, which are stabilized by interactions between the large AAA+ domain of one subunit and the small AAA+ domain of its neighbor[2]. A hinge-linker connects the large and small AAA+ domains of each subunit (Fig. 1A).

ClpX is a hexameric AAA+ protein unfoldase that is present in most bacteria and some eukaryotic organelles. It unfolds specific proteins, including those that are mistranslated or damaged, and feeds the unfolded polypeptide into an internal chamber of the associated ClpP peptidase for proteolysis[3]. Recognition of appropriate substrates is mediated by sequence motifs (degrons) that target proteins to ClpX either directly or with the help of adapter proteins. In *Escherichia coli*, the 11-residue ssrA degron is appended to the C-terminus of partially synthesized proteins on stalled ribosomes, and ClpXP or other cellular proteases degrade the resulting ssrA-tagged polypeptides[4–7]. The ssrA tag initially binds to loops within the axial pore of the hexameric ClpX ring[8–9]. Conformational changes in the pore — driven by ATP binding, hydrolysis, and product release — then pull on the tag, eventually resulting in unfolding and stepwise translocation into ClpP for degradation[10–13].

In crystal structures, the hexameric ClpX ring is stabilized by relatively invariant rigid-body interactions between the large and small AAA+ domains of neighboring subunits[14–15] (Fig. 1A). Moreover, covalent crosslinks across these rigid-body interfaces do not compromise ClpXP degradation activity, indicating that these contacts are maintained during the conformational rearrangements in the hexamer that drive substrate unfolding and translocation[16]. Consequently, the enzyme motions responsible for mechanical work are proposed to arise from changes in the orientations of neighboring rigid bodies, which are mediated in turn by structural changes in the four-residue linkers that connect the large and

small AAA+ domains of each subunit and function as hinges between successive rigid bodies[14–16].

Mutant ClpX rings with only a single subunit capable of hydrolyzing ATP support low levels of ClpP degradation[17], indicating that unfolding and translocation do not require sequential or concerted ATP hydrolysis. Although ClpX hydrolyzes many molecules of ATP while attempting to unfold a stable protein substrate, cooperative unfolding ultimately occurs as a consequence of a power stroke driven by a single hydrolysis event[10–13,18–19]. Robust unfolding requires coordination between the axial-pore loops of multiple ClpX subunits[20-22]. Moreover, ATP hydrolysis by ClpX is positively cooperative, implying some means of subunit-subunit communication[23]. Evidence of intersubunit communication is also observed in the enzyme's mechanical activity. Although the smallest translocation steps taken by ClpXP are ~1 nm in length, kinetic bursts of ATP hydrolysis appear to be responsible for steps of approximately 2, 3, and 4 nm[12–13]. Such communication could arise from contacts between neighboring large AAA+ domains and/or through the hinge-linkers that control the orientation of neighboring rigid bodies.

The hinge-linkers of ClpX form part of the ATP binding site. In *E. coli* ClpX, a conserved hinge-linker residue (L317) contacts nucleotide in crystal structures[14]. The sequence of the rest of the four-residue hinge-linker is poorly conserved but its length is important, as insertion or deletion of one residue in all six hinge-linkers of a hexamer severely impairs unfolding activity but not ATP hydrolysis[16]. To better understand the roles of the ClpX hinge-linkers in intersubunit communication during substrate unfolding, we have used circular permutation to delete one or more hinge-linkers and engineered linker-disruption and ATP-hydrolysis mutations to interrogate how the hinge-linkers affect ClpX function. Our results support a model in which the hinge-linkers facilitate communication between subunits both by enforcing closed-ring topology and maintaining proper subunit-subunit geometry within the ring during ATP hydrolysis.

## Materials and Methods

### Protein expression and purification

$ClpX^{\Delta N}$ (residues 62-424) constructs were expressed and purified as described[17]. Linker-deletion $ClpX^{\Delta N}$ was produced by circularly permuting covalently tethered $ClpX^{\Delta N}$ constructs using Gibson Assembly (New England Biolabs). The G12-insertion was introduced into one hinge-linker of a $ClpX^{\Delta N}$ pseudohexamer[17] after residue N315 using PCR mutagenesis. Arc-st11-ssrA, Arc-Gcn4-st11-ssrA, GFP-ssrA, and $^{CP7}$GFP-ssrA substrates were purified as described[18,23,24].

### Linkerless ClpX assembly assays

The oligomeric state of linker-deletion constructs was determined by analytical size-exclusion chromatography at 4°C. Protein samples were diluted to 3 μM (hexamer equivalents) and 200 μL was injected onto a Superdex-200 10/300 column (GE Healthcare) equilibrated in buffer A (25 mM HEPES-KOH, pH 7.5, 5 mM $MgCl_2$, 200 mM KCl, 10% glycerol) supplemented with 1 mM ADP.

ClpX$^{\Delta N}$ hexamers were analyzed using negative-stain electron microscopy performed by Nicki Watson (W.M. Keck Microscopy Facility, Whitehead Institute, MIT). Freshly-ionized 200-mesh Cu/carbon grids were floated on 10 μL drops of protein sample for ~60 s. The grids were then blotted dry, washed with 1% aqueous uranyl acetate, and blotted dry again. Grids were imaged at 100 kV on a Technai Spirit Transmission Electron Microscope (FEI). Electron micrographs were class averaged using RELION 2.0 software[25]. For the wild-type, G12-insertion, and linker-deletion variants imaged, 641, 792, and 1287 particles, respectively, were manually selected at 100 pixel diameter from micrographs taken at 49,000-fold (wild-type and linker-deletion) or 98,000-fold (G12-insertion) magnification. The length-to-pixel ratio was increased two-fold for the higher-magnification G12-insertion micrographs to facilitate consistent downstream analysis. For the wild-type and G12-insertion constructs, in which the particles appear as compact rings, an 80-pixel opaque circular mask was applied to each particle, and particles were averaged into four classes. For the linker-deletion construct, a 100-pixel mask was applied, and particles were averaged into 10 classes to accommodate the less compact and more heterogeneous nature of these particles.

## Biochemical assays

Activity assays were carried out at 30°C in buffer PD (25 mM HEPES-KOH, pH 7.5, 35 mM $MgCl_2$, 200 mM KCl, 10% glycerol). Kinetics were analyzed using Prism 7 (GraphPad). ATP hydrolysis was measured using a coupled-NADH oxidation assay as described[17]. ClpP binding assays were performed using the protocol and RseA fluorogenic decapeptide substrate described[26]. Solution unfolding was assayed using a FRET-based unfolding assay as described[24].

GFP-ssrA and $^{CP7}$GFP-ssrA degradation assays were performed by measuring loss of GFP fluorescence (excitation 467 nm; emission 511 nm) using a SpectraMax M5 plate reader (Molecular Devices). For fluorescence-based Arc-st11-ssrA degradation assays, purified Arc-st11-ssrA was labeled with a 10-fold molar excess of NHS-Fluorescein (ThermoFisher) in Buffer B (25 mM HEPES-KOH, pH 7.5, 300 mM KCl, 10% glycerol, 1 mM dithiothreitol [DTT]) for 45 min at ambient temperature. The reaction was quenched with an excess of Tris-HCl (pH 7.6), and the labeled protein was separated from free dye and desalted into Buffer A over a Superdex-75 16/600 column (GE Healthcare). Because Arc-st11-ssrA has six lysine residues, multiple labeling with fluorescein caused label molecules on the same substrate to mutually quench fluorescence emission. Substrate degradation by ClpXP was monitored by increased fluorescence (excitation 480 nm; emission 525 nm) using a SpectraMax M5 plate reader (Molecular Devices). Endpoint fluorescence was measured after adding an excess of trypsin to the reaction, and the amount of Arc-st11-ssrA degraded was calculated from the initial and final fluorescence values. Because each preparation of substrate was labeled to a different extent, we observed ~30% batch-to-batch variability in apparent degradation rate by the same prep of ClpXP. To prevent invalid comparison of rates between batches, we included appropriate controls in each experiment and reported Arc-st11-ssrA degradation activity relative to a wild-type ClpX$^{\Delta N}$ construct where practical.

For degradation efficiency experiments, ATP hydrolysis and substrate degradation activity were measured as a function of substrate concentration, and the resulting responses were fit to hyperbolic functions to obtain $V_{max}$ values for the rates of ATP hydrolysis and substrate degradation at saturating substrate. In cases where the ATP hydrolysis rate was unresponsive to increasing concentrations of substrate, a constant linear fit was used. To calculate mechanical efficiency, $V_{max}$ for ATP hydrolysis was divided by $V_{max}$ for substrate degradation.

### Crosslinking

A variant of linker-deletion $ClpX^{\Delta N}$ pseudohexamer with cysteine residues on either side of the deleted hinge-linker interface was mixed with a 100-fold excess of a Cys-free *E. coli* ClpP variant (C91V/C113A). The protein mixture was desalted into PD buffer using G25 resin (GE Healthcare) to remove DTT. The desalted protein was separated into two pools, and 2 mM ATPγS was added to each pool. Either 1,11-bismaleimido-triethyleneglycol (Thermo Scientific) or equal maleimide equivalents of N-propyl-maleimide (Sigma) was then added. The maleimide agents were added in 1:1 stoichiometry with sulfhydryl groups on $ClpX^{\Delta N}$, and DMSO cosolvent was added to 12% of the reaction volume. The reactions were allowed to proceed for 1 hour at 30°C, then quenched with 1 mM DTT for 15 min at 30°C. The reactions were again desalted into PD buffer over PD-10 columns (GE Healthcare), and concentrated with centrifugal concentrators (Millipore-Sigma). Reactions were normalized by total protein using a Bradford assay prior to measuring degradation activity (Thermo Scientific). To gauge crosslinking efficiency, equal volumes of each reaction were separated on a 10% bis-tris SDS-polyacrylamide gel run at 120V in MES buffer, stained with Coomassie Brilliant Blue, and imaged.

## Results

### Mutating or deleting a single hinge-linker impairs intersubunit communication

To determine whether a ClpX hexamer requires six hinge-linkers for robust function, we used circular permutation to create a single-chain pseudohexamer missing one hinge-linker (Fig. 1B). Prior studies show that single-chain pseudohexamers of $ClpX^{\Delta N}$, in which the wild-type N-terminal domain is deleted, have activities similar to wild-type ClpX hexamers in supporting degradation of ssrA-tagged substrates by ClpP[17]. As shown in Fig. 1B, moving the large domain of the N-terminal subunit of a single-chain pseudohexamer to the end of the C-terminal small domain results in a linker-deletion variant missing one hinge-linker. To compare the effects of deleting versus mutationally disrupting a hinge-linker, we also constructed a non-permuted pseudohexamer in which 12 glycine residues were inserted into a single hinge-linker (G12 insertion, Fig. 1C). During purification, both the linker-deletion and G12-insertion variants eluted from a size-exclusion column at positions expected for hexamers (Fig. 1D), establishing that these hinge-linker mutations do not cause multimeric aggregation.

ATP hydrolysis by ClpX is positively cooperative[27]. We measured the ATP dependence of hydrolysis for the parental pseudohexamer and the linker-deletion and G12-insertion variants and fit the resulting data to the Hill form of the Michaelis-Menten equation (Fig. 2A, Table

1). Compared to the parental pseudohexamer, both linker-disruption mutants had ~3-fold higher $V_{max}$ values and ~5-7-fold higher apparent $K_M$ values. The Hill constant was ~2.0 for the parent, ~1.6 for the linker-deletion variant, and ~1.1 for the G12-insertion enzyme (Fig. 2A, Table 1). Hence, the hinge-linker disruptions affect many aspects of steady-state ATP hydrolysis, including communication between subunits that results in positive cooperativity. Addition of ClpP repressed ATP hydrolysis by all three variants, although this effect was only observed in the linker-deletion variant at high concentrations of ClpP (Fig. 2B, Supp. Fig. 1). Addition of an Arc-st11-ssrA protein substrate and ClpP stimulated ATP hydrolysis by the parental and G12-insertion enzymes but had little effect on the linker-deletion variant, even at high ClpP and substrate concentrations (Fig. 2B, Supp. Fig. 1).

We assayed the ability of the parental pseudohexamer, the linker-deletion variant, and the G12-insertion variant to support ClpP degradation of 15 μM Arc-st11-ssrA (Fig. 2C). The G12-insertion variant supported ClpP degradation at ~25% of the parental rate, whereas the linker-deletion variant supported degradation at less than 1% of the parental rate. We also measured proteolysis activity against $^{CP7}$GFP-ssrA and GFP-ssrA, which are incrementally more difficult to unfold and degrade[23]. The G12-insertion variant supported ClpP degradation of these substrates at lower rates than the wild-type pseudohexamer, but the linker-deletion variant did not appreciably degrade either of these more-stable substrates (Fig. 2D) Thus, deletion of a single hinge-linker dramatically reduces degradation activity, whereas mutational insertion diminishes activity far less severely across a range of substrate stabilities.

In principle, poor binding to the ssrA-tagged substrate or to ClpP could be responsible for the reduced degradation activities of the hinge-linker variants. To test substrate binding, we assayed degradation rates as a function of the concentration of Arc-st11-ssrA (Fig. 2E, Table 1). The parental enzyme and the G12-insertion variant had Km values for the protein substrate within ~2-fold, whereas Km for the linker-deletion variant increased significantly. To assay ClpP binding, we took advantage of the fact that ClpX activates ClpP degradation of a small peptide substrate by opening the axial pore[28]. The parental and G12-insertion enzymes bound ClpP with low nanomolar affinities in this assay, whereas the linker-deletion variant bound with an affinity of ~750 nM (Fig. 2F, Table 1). Thus, the presence of all six hinge-linkers appears to be required for robust interaction between ClpX and ClpP.

Because the linker-deletion pseudohexamer appeared to have low affinity for ClpP, we were concerned that our measurements could underestimate degradation rates because they were performed at concentrations of ClpP below the $K_D$ measured by pore opening. To test this model directly, we compared rates of degradation of 15 μM Arc-st11-ssrA by the linker-deletion pseudohexamer in the presence of different concentrations of ClpP (Supp. Fig. 2A). The apparent affinity was substantially higher in this assay, and the linker-deletion pseudohexamer was largely saturated in degradation assays performed in the presence of 300 nM $ClpP_{14}$ (Supp. Fig. 2B). Although we do not know why the pore-opening and degradation assays give different affinities, one possibility is that the presence of a protein substrate strengthens the interaction between ClpX and ClpP.

We also assayed rates of ATP hydrolysis in the presence of ClpP and increasing concentrations of Arc-st11-ssrA (Fig. 2G, Table 1), which stimulated ATP hydrolysis by the parental enzyme and G12-insertion variant but had no significant effect on the linker-deletion variant. The maximal rate of ATP hydrolysis at saturating Arc-st11-ssrA divided by $V_{max}$ for substrate degradation provides an estimate of the ATP cost of degradation (Fig. 2H). Degradation of one Arc-st11-ssrA protein required hydrolysis of ~110 ATPs by the parental enzyme and ~290 ATPs by the G12-insertion variant. Although weak interaction with substrate precluded precise determination of the $V_{max}$ for substrate degradation by the linker-deletion variant, extrapolating the fitted curve suggests a bulk energy cost of ~2000 ATPs, substantially higher than either the parental or G12-insertion variants. These results support a model in which hinge-linker deletion or disruption reduce the mechanical efficiency of ClpX to different extents, either because many power strokes fail or because ATP hydrolysis and power strokes are uncoupled.

## Hinge-linkers facilitate formation of closed rings

ClpX functions as a topologically closed ring[16]. In negative-stain electron microscopy, the parental pseudohexamer and G12-insertion variant exclusively showed ring structures in 2D class averages (Figs. 3A, 3B). By contrast, the linker-deletion variant (Fig. 3C) displayed a mixture of C-shaped open structures (~55%), twisted shapes that did not classify discreetly (~5%), and rings (~40%). The last value should be viewed as an upper bound, as some particles that appear as rings in projection could be open in three dimensions. This mixture of open- and closed-ring structures suggests that a stable closed-ring conformation is unlikely to be the dominant conformation of the linker-deletion variant.

## Multiple hinge-linker deletions prevent stable hexamer assembly

To test whether deletion of multiple hinge-linkers increases the severity of the mechanical defects observed for the linker-deletion variant, we constructed a circularly permuted $ClpX^{\Delta N}$ monomer (no hinge-linker), a circularly permuted single-chain dimer (one hinge-linker; similar to a variant characterized in ref. 15), and a circularly permuted single-chain trimer (two hinge-linkers) as shown in Fig. 4A. In size-exclusion chromatography experiments in the presence of ADP, which stabilizes assembly of $ClpX^{\Delta N}$ hexamers, these purified linker-deletion variants eluted at positions expected for monomers, dimers, and trimers (Fig. 4B). Because non-permuted single-chain $ClpX^{\Delta N}$ dimers and trimers assemble into pseudohexamers[17], the hinge-linker deletions clearly compromise stable hexamer formation. Rates of basal ATP hydrolysis increased in rough proportion to the number of hinge-linkers in each variant (Fig. 4C). None of the variants tested exhibited significant increases in hydrolysis rate in response to Arc-st11-ssrA substrate, and only linker-deletion single-chain hexamer exhibited hydrolysis repression in the presence of ClpP. The severe hydrolysis defect of the monomeric linker-deletion variant is not surprising, as side chains from neighboring subunits are required to form the wild-type active site for ATP hydrolysis[14].

We used a FRET-based Arc-Gcn4-ssrA unfolding assay[24] to measure substrate denaturation by different linker-deletion variants in the absence of ClpP (Fig. 4D). The linker-deletion dimer and turner displayed no detectable unfolding, whereas the linker-deletion hexamer

displayed less than 1% of the activity of wild-type ClpX$^{\Delta N}$. In the presence of ClpP, low levels of degradation activity were observed for the linker-deletion dimer and trimer (Fig. 4E), suggesting that ClpP can promote unfolding by serving as a scaffold for hexamer assembly. Interestingly, the ClpP degradation activities of the linker-deletion dimer (three missing hinge-linkers per hexamer) and trimer (two missing hinge-linkers per hexamer) were roughly 30% and 50%, respectively, of that of the circularly permuted hexamer (one missing hinge-linker per hexamer). Hence, although deletion of a single hinge-linker causes a ~100-fold decrease in degradation activity, additional deletions cause degradation defects roughly proportional to the number of missing hinge-linkers (Fig. 4F). To exclude the possibility that the low degradation activities of the linker-deletion variants might result from ATP-independent degradation, we tested degradation in the presence of ATP$\gamma$S, an ATP analog hydrolyzed very slowly by ClpX[29]. Under these conditions, the linker-deletion variants did not support detectable levels of ClpP-mediated degradation, confirming that degradation results from ClpX mechanical activity (Fig. 4E).

## Re-closing a broken hinge-linker interface improves mechanical activity

Because the linker-deletion pseudohexamer degrades substrates slowly and inefficiently and often adopts open-ring conformations, we asked whether covalently re-closing the ring would restore mechanical activity. To permit crosslinking, we engineered a variant with Cys-Leu and Leu-Cys residues at the N- and C-terminal ends of the pseudohexamer, respectively (dual-Cys ClpX$^{\Delta N}$, Fig. 5A), and saturated the reaction with ClpP with the aim of bringing the terminal Cys residues into proximity for crosslinking. We mixed dual-Cys ClpX$^{\Delta N}$ with 1,11-bismaleimido-triethyleneglycol (BM-PEG$_3$, a bifunctional maleimide crosslinker with an 18 Å flexible spacer) in the presence of a 100-fold excess of a Cys-free ClpP$_{14}$ variant and ATP$\gamma$S (Fig. 5A). To control for nonspecific effects of sulfhydryl modification, a parallel reaction was treated with N-propyl-maleimide (NPM), a monofunctional maleimide crosslinker (Fig. 5A). After crosslinking, a supershifted ClpX band was observed only in the BM-PEG$_3$ reaction, consistent with covalent circularization of the ClpX pseudohexamer[15] (Fig. 5B). Compared to the NPM-modified enzyme, dual-Cys ClpX$^{\Delta N}$ treated with BM-PEG$_3$ supported substantially faster ClpP degradation of Arc-st11-ssrA (Fig. 5C) and $^{CP7}$GFP-ssrA (Fig. 5D). The hinge-linkers therefore contribute to robust degradation by enforcing a closed-ring topology.

## Functional asymmetry relative to the position of a hinge-linker mutation

To better understand how the hinge-linkers transmit information between ClpX subunits, we constructed single-chain hexamers with Walker-B ATP-hydrolysis mutations in three subunits counter-clockwise (FAB$_{EQ}$) or clockwise (DEF$_{EQ}$) from a G12 hinge-linker insertion (when viewed from the substrate binding face; Fig. 6A). $V_{max}$ for ClpP degradation of Arc-st11-ssrA was reduced for both variants compared to the G12-insertion parent, but the DEF$_{EQ}$ variant was about twice as active as the FAB$_{EQ}$ variant (Fig. 6B, Table 1). However, the maximal rate of ATP hydrolysis was higher for FAB$_{EQ}$ than for DEF$_{EQ}$ in the presence of ClpP and Arc-st11-ssrA (Fig. 6C, Table 1). Indeed, the G12 parent hydrolyzed an average of 210 ATPs per Arc-st11-ssrA degraded, whereas the cost was 450 ATPs for DEF$_{EQ}$ and 2400 ATPs for FAB$_{EQ}$ (Fig. 6D). Thus, the hinge-linker insertion is less

deleterious when it is clockwise from two wild-type subunits than when it is counter-clockwise.

## Discussion

The mechanical functions of the ClpX ring depend upon conformational rearrangements driven by ATP binding and hydrolysis. Hinge-linkers that connect the large and small AAA+ domains of each subunit in the hexamer appear to be the primary sites of flexibility that allow conformational motion within the ring[14,16]. However, it was unclear previously how the hinge-linkers contribute to ATP hydrolysis and substrate unfolding by ClpX. The present work identifies two distinct roles for these elements in facilitating intersubunit communication and robust unfolding activity.

Several experiments reveal a major role of the hinge-linkers in maintaining closed hexameric rings. As assayed by electron microscopy, deleting one hinge-linker in a hexamer allows a majority of molecules to adopt open-ring conformations. The ability to form and maintain a topologically closed ring also correlates with robust ClpX function. Deletion of one hinge-linker prevents ClpXP degradation of stable protein substrates and dramatically slows proteolysis of less stable substrates, and deletion of multiple hinge-linkers abrogates hexamer assembly and mechanical function. Insertion of a flexible 12-glycine sequence into a single hinge-linker of a hexamer resulted in less severe functional defects than those associated with deleting a hinge-linker. Similarly, the proteolysis defects of the single hinge-linker deletion were partially rescued by a chemical crosslink that restored covalent connectivity.

The hinge-linkers play a second important role facilitating communication and regulating activity within the closed ClpX ring. We find that insertion of 12 glycines into a single hinge-linker increases the maximal velocity of ATP hydrolysis, reduces the positive cooperativity of hydrolysis with respect to ATP concentration, and substantially increases the average number of ATP hydrolysis events required for degradation of one substrate. Interestingly, inserting 12 glycines into a hinge-linker within the context of the closed ring decreases ATP hydrolysis cooperativity to a greater extent than the open-ring hinge-linker deletion, suggesting that hinge-linker length may be optimized for intersubunit communication within a closed-ring topology. We conclude that the wild-type hinge-linkers contribute to regulation of basal ATP hydrolysis rate and efficiently couple ATP hydrolysis with the mechanical processes needed for protein unfolding and translocation. Previous studies reinforce this conclusion, as single-residue insertions or deletions in all six ClpX hinge-linkers also reduce the rate of degradation and increase the ATP cost[16]. Because disrupting a single hinge-linker is phenotypically similar to disrupting all six, the hinge-linkers may mediate long-range communication between subunits within the ring. A mechanism in which conformational changes in one subunit are sensed by all other subunits via tension transmitted through the hinge-linkers is consistent with this model of intersubunit communication.

Compared to the parent or G12 insertion, the single hinge-linker deletion weakened ClpX affinity for ClpP and protein substrates, suggesting that a stable closed ring is needed for

optimal binding. Structures of ClpP reveal that its ClpX-interacting surface is planar[30]. In an open-ring structure, some of the ClpX loops that normally interact with clefts on the ClpP surface are unlikely to make productive contacts[31-33]. In support of this model, a previous study demonstrates that deleting one of the six loops that interact with ClpP from a single-chain ClpX pseudohexamer weakens ClpP interaction ~50-fold[32], whereas our hinge-linker deletion variant has a ~35-fold binding defect as measured by ClpP pore opening. Furthermore, ClpP may function as a scaffold for proper ClpX geometry, enforcing a ring-hexamer conformation. Linker-deletion single-chain dimers and trimers, which do not detectably unfold substrates on their own, support low levels of ClpP-mediated substrate degradation. Additionally, both linker-deletion and G12-insertion single-chain hexamer variants exhibit high levels of ATP hydrolysis on their own, but this activity is repressed to near-parental levels when sufficient ClpP is added. It seems likely that ClpX must adopt a ring-hexamer topology to productively interact with ClpP, and that the weakened affinity of the linker-deletion variant for ClpP reflects the entropic penalty of constraining it to a closed-ring conformation.

Loss of coordinated contacts from multiple subunits could also explain the substrate-binding defect of the single hinge-linker deletion variant. Residues in the axial-pore-1 loops of ClpX are important for binding of ssrA-tagged substrates, and mutating increasing numbers of these pore loops increases $K_M$ for substrate degradation[8–9,20–22]. Similar to the observed ClpP binding defect, substrate binding may be impaired in the linker-deletion pseudohexamer because the open-ring conformation prevents pore-1 loops on either side of the broken interface from coordinating grip and unfolding activity during substrate processing.

We find that placing Walker-B ATP hydrolysis mutations on one side or the other of a disrupted hinge-linker results in an approximate 5-fold difference in the average number of ATPs required to degrade a single substrate. This result suggests that communication between subunits in the ClpX hexamer occurs with some directional bias. Single-molecule studies indicate that kinetic bursts of power strokes from multiple ClpX subunits contribute to mechanical activity[10–13,19]. Thus, asymmetry relative to a disrupted hinge-linker could arise if conformational changes are communicated more efficiently through a wild-type hinge-linker on its clockwise side, allowing coordinated action of more subunits during each unfolding power stroke. However, axial pore contacts from multiple subunits also contribute to substrate grip and thus to unfolding efficiency[20–22], and the observed asymmetry could also arise from directional effects on grip.

Many recent structures of ATP-dependent protein translocation motors show the six subunits of each hexamer in a spiral staircase topology[34–37]. The asymmetric nature of these structures has led to proposed mechanisms in which subunits hydrolyze ATP sequentially, facilitating hand-over-hand substrate translocation[35–37]. A recent study using cryo EM single-particle analysis identified classes in which ATP was bound to different sets of protomers within the $Rpt_{1-6}$ motor, which could represent intermediates in a rotary hydrolysis and translocation mechanism[38]. However, ClpX has been shown to hydrolyze ATP and translocate substrates via a probabilistic rather than sequential mechanism[13,17], and several other AAA+ unfoldases are also unlikely to be constrained to a sequential mode of

action[39,40]. Our observation of functional asymmetry relative to a hinge-linker disruption is consistent with a hybrid model in which ClpX operates most efficiently when bursts of ATP hydrolysis initiate stochastically, but subsequent hydrolysis events are biased toward a sequential, unidirectional mode of action.

The principles identified for hinge-linkers in ClpX may be broadly applicable to other protein unfolding motors. The AAA+ protein unfoldases HslU, FtsH, Yme1, PAN, ClpA, ClpB, Hsp104, Cdc48/p97, and the $Rpt_{1-6}$ ring of the proteasome all share conserved large and small domains connected by a hinge-linker. The sequence of the ClpX hinge-linker region is poorly conserved in proteobacteria but its length is invariant[16]. In annotated crystal structures of AAA+ unfoldases from multiple clades, the hinge-linkers are also 4-5 amino acids in length. This possible evolutionary constraint on hinge-linker length suggests that defined length is an important determinant of function for most, if not all, AAA+ protein remodeling machines.

## Conclusions

In conclusion, we have characterized the structural and functional impacts of deleting or disrupting a single hinge-linker element in the ClpX protein unfolding motor. Deleting one hinge-linker prevents ring-hexamer assembly and causes defects in substrate unfolding, ATP hydrolysis cooperativity, and ClpP binding. Mutational insertion of 12 glycines into a hinge-linker preserves closed-ring structure, but impairs substrate unfolding and ATP hydrolysis cooperativity. We further validated the significance of the closed ring structure by demonstrating that covalently reclosing a broken hinge-linker interface partially restores substrate unfolding activity. Finally, we report an asymmetry in ClpX degradation efficiency when a hinge-linker mutation is placed on either side of hydrolysis-defective subunits, suggesting biased directional effects on grip or intersubunit communication through the hinge-linkers.

## Supplementary Material

Refer to Web version on PubMed Central for supplementary material.

## Acknowledgments

This work was supported by US National Institutes of Health (NIH) grant GM-101988 (R.T.S.). T.A. Bell was supported in part by US NIH grant 5T32GM-007287. T.A. Baker is an employee of the Howard Hughes Medical Institute. We thank Nicki Watson and Xue Fei for help with microscopy and downstream analysis; Steven Glynn, Karl Schmitz, Sanjay Hari, and Juhee Park for helpful discussions; and members of the Sauer and Baker labs for providing feedback on the manuscript.

## References

1. Erzberger Jan P., and Berger James M. (2006) Evolutionary relationships and structural mechanisms of AAA+ proteins, Annu. Rev. Biophys. Biomol. Struct 35, 93–114. [PubMed: 16689629]
2. Hanson Phyllis I. and Whiteheart Sidney W. (2005) AAA+ proteins: have engine, will work, Nat. Rev. Mol. Cell. Biol 6, 519–529. [PubMed: 16072036]
3. Sauer Robert T. and Baker Tania A. (2011) AAA+ proteases: ATP-fueled machines of protein destruction, Annu. Rev. Biochem 80, 587–612. [PubMed: 21469952]

4. Keiler Kenneth C., Waller Patrick R.H., and Sauer Robert T. (1996) Role of a peptide tagging system in degradation of proteins synthesized from damaged messenger RNA, Science 271, 990–993. [PubMed: 8584937]
5. Gottesman Susan, Roche Eric, Zhou YanNing, and Sauer Robert T. (1998) The ClpXP and ClpAP proteases degrade proteins with carboxy-terminal peptide tails added by the SsrA-tagging system, Genes Dev. 12, 1338–1347. [PubMed: 9573050]
6. Choy Jennifer S., Aung Latt Latt, and Karzai, A. Wali. (2007) Lon protease degrades transfer-messenger RNA-tagged proteins, J. Bacteriol 189, 6564–6571. [PubMed: 17616591]
7. Hari Sanjay B. and Sauer Robert T. (2016) The AAA+ FtsH protease degrades an ssrA-tagged model protein in the inner membrane of Escherichia coli, Biochemistry 55, 5649–5652. [PubMed: 27677373]
8. Siddiqui Samia M., Sauer Robert T., and Baker Tania A. (2004) Role of the processing pore of the ClpX AAA+ ATPase in the recognition and engagement of specific protein substrates, Genes Dev. 18, 369–374. [PubMed: 15004005]
9. Martin Andreas, Baker Tania A., and Sauer Robert T. (2008) Pore loops of the AAA+ ClpX machine grip substrates to drive translocation and unfolding, Nat. Struct. Mol. Biol 15, 1147–1151. [PubMed: 18931677]
10. Aubin-Tam Marie-Eve, Olivares Adrian O., Sauer Robert T., Baker Tania A., and Lang Matthew J. (2011) Single-molecule protein unfolding and translocation by an ATP-fueled proteolytic machine, Cell 145, 257–267. [PubMed: 21496645]
11. Maillard Rodrigo A., Chistol Gheorghe, Sen Maya, Righini Maurizio, Tan Jiongyi, Kaiser Christian M., Martin Andreas, Bustamante Carlos. (2011) ClpX(P) generates mechanical force to unfold and translocate its protein substrates, Cell 145, 459–469. [PubMed: 21529717]
12. Sen Maya, Maillard Rodrigo A., Nyquist Kristofor, Rodriguez-Aliaga Piere, Presse Steve, Martin Andreas, and Bustamante Carlos (2013) The ClpXP protease unfolds substrates using a constant rate of pulling but different gears, Cell 155, 636–646. [PubMed: 24243020]
13. Cordova Juan Carlos, Olivares Adrian O., Shin Yongdae, Stinson Benjamin M., Calmat Stephane, Schmitz Karl R., Aubin-Tam Marie-Eve, Baker Tania A., Lang Matthew J., and Sauer Robert T. (2014) Stochastic but highly coordinated protein unfolding and translocation by the ClpXP proteolytic machine, Cell 158, 647–658. [PubMed: 25083874]
14. Glynn Steven E., Martin Andreas, Nager Andrew R., Baker Tania A., and Sauer Robert T. (2009) Structures of asymmetric ClpX hexamers reveal nucleotide-dependent motions in a AAA+ protein-unfolding machine, Cell 139, 744–756 [PubMed: 19914167]
15. Stinson Benjamin M., Nager Andrew R., Glynn Steven E., Schmitz Karl R., Baker Tania A., and Sauer Robert T. (2013) Nucleotide binding and conformational switching in the hexameric ring of a AAA+ machine, Cell 153, 628–639. [PubMed: 23622246]
16. Glynn Steven E., Nager Andrew R., Baker Tania A., and Sauer Robert T. (2012) Dynamic and static components power unfolding in topologically closed rings of a AAA+ proteolytic machine, Nat. Struct. Mol. Biol 19, 616–622. [PubMed: 22562135]
17. Martin Andreas, Baker Tania A., and Sauer Robert T. (2005) Rebuilt AAA+ motors reveal operating principles for ATP-fuelled machines, Nature 437, 1115–1120. [PubMed: 16237435]
18. Kenniston Jon A., Baker Tania A., Fernandez Julio M., and Sauer Robert T. (2003) Linkage between ATP consumption and mechanical unfolding during the protein processing reactions of an AAA+ degradation machine, Cell 114, 511–520. [PubMed: 12941278]
19. Olivares Adrian O., Kotamarthi Hema Chandra, Stein Benjamin J., Sauer Robert T., and Baker Tania A. (2017) Effect of directional pulling on mechanical protein degradation by ATP-dependent proteolytic machines, Proc. Natl. Acad. Sci. U. S. A 114, E6306–E6313. [PubMed: 28724722]
20. Iosefson Ohad, Nager Andrew R., Baker Tania A., and Sauer Robert T. (2015) Coordinated gripping of substrate by subunits of a AAA+ proteolytic machine, Nat. Chem. Biol 11, 201–206. [PubMed: 25599533]
21. Iosefson Ohad, Olivares Adrian O., Baker Tania A., and Sauer Robert T. (2015) Dissection of axial-pore loop function during unfolding and translocation by a AAA+ proteolytic machine, Cell Rep. 12, 1032–1041. [PubMed: 26235618]

22. Rodriguez-Aliaga Piere, Ramirez Luis, Kim Frank, Bustamante Carlos, and Martin Andreas. (2016) Substrate-translocating loops regulate mechanochemical coupling and power production in AAA+ protease ClpXP, Nat. Struct. Mol. Biol 23, 974–981. [PubMed: 27669037]
23. Nager Andrew R., Baker Tania A., and Sauer Robert T. (2011) Stepwise unfolding of a β barrel protein by the AAA+ ClpXP protease, J. Mol. Biol 413, 4–16. [PubMed: 21821046]
24. Baytshtok Vladimir, Baker Tania A., and Sauer Robert T. (2015) Assaying the kinetics of protein denaturation catalyzed by AAA+ unfolding machines and proteases, Proc. Natl. Acad. Sci. U. S. A 112, 5377–5382. [PubMed: 25870262]
25. Scheres Sjors H.W. (2012) RELION: implementation of a bayesian approach to cryo-EM structure determination, J. Struc. Biol 180, 519–530.
26. Lee Mary E., Baker Tania A., and Sauer Robert T. (2010) Control of substrate gating and translocation into ClpP by channel residues and ClpX binding, J. Mol. Biol 399, 707–718. [PubMed: 20416323]
27. Hersch Greg L., Burton Randall E., Bolon Daniel N., Baker Tania A., and Sauer Robert T. (2005) Asymmetric interactions of ATP with the AAA+ $ClpX_6$ unfoldase: allosteric control of a protein machine, Cell 121, 1017–1027. [PubMed: 15989952]
28. Grimaud Regis, Kessel Martin, Beuron Fabienne, Steven Alasdair C., and Maurizi Michael R. (1998) Enzymatic and structural similarities between the Escherichia coli ATP-dependent proteases, ClpXP and ClpAP, J. Biol. Chem 273, 12476–12481. [PubMed: 9575205]
29. Burton Randall E., Baker Tania A., and Sauer Robert T. (2003) Energy-dependent degradation: linkage between ClpX-catalyzed nucleotide hydrolysis and protein-substrate processing, Protein Sci. 12, 893–902. [PubMed: 12717012]
30. Wang Jimin, Hartling James A., and Flanagan John M. (1997) The structure of ClpP at 2.3 Å resolution suggests a model for ATP-dependent proteolysis, Cell 91, 447–456. [PubMed: 9390554]
31. Kim Yong-In, Levchenko Igor, Fraczkowska Karolina, Woodruff Rachel V., Sauer Robert T., and Baker Tania A. (2001). Molecular determinants of complex formation between Clp/Hsp100 ATPases and the ClpP peptidase, Nat. Struct. Mol. Biol 8, 230–233.
32. Martin Andreas, Baker Tania A., and Sauer Robert T. (2007) Distinct static and dynamic interactions control ATPase-peptidase communication in a AAA+ protease, Mol. Cell 27, 41–52. [PubMed: 17612489]
33. Amor Alvaro J., Schmitz Karl R., Sello Jason K., Baker Tania A., and Sauer Robert T. (2016) Highly dynamic interactions maintain kinetic stability of the ClpXP protease during the ATP-fueled mechanical cycle, ACS Chem. Biol 11, 1552–1560. [PubMed: 27003103]
34. Lander Gabriel C., Estrin Eric, Matyskiela Mary E., Bashore Charlene, Nogales Eva, and Martin Andreas. (2012) Complete subunit architecture of the proteasome regulatory particle, Nature 482, 186–191. [PubMed: 22237024]
35. Monroe Nicole, Han Han, Shen Peter S., Sundquist Wesley I., and Hill Christopher P. (2017) Structural basis of protein translocation by the Vps4-Vta1 AAA ATPase, eLife 6, e24487. [PubMed: 28379137]
36. Gates Stephanie N., Yokom Adam L., Lin JiaBei, Jackrel Meredith E., Rizo Alexandrea N., Kendsersky Nathan M., Buell Courtney E., Sweeny Elizabeth A., Mack Korrie L., Chuang Edward, Torrente Mariana P., Su Min, Shorter James, and Southworth Daniel R. (2017) Ratchet-like polypeptide translocation mechanism of the AAA+ disaggregase Hsp104, Science 357, 273–279. [PubMed: 28619716]
37. Puchades Cristina, Rampello Anthony J., Shin Mia, Giuliano Christopher J., Wiseman R. Luke, Glynn, Steven E., and Lander Gabriel C. (2017) Structure of the mitochondrial inner membrane AAA+ protease YME1 gives insight into substrate processing, Science 358, eaao0464. [PubMed: 29097521]
38. Eisele Markus R., Reed Randi G., Rudack Till, Schweitzer Andreas, Beck Florian, Nagy Istvan, Pfeifer Gunter, Plitzko Jürgen M., Baumeister Wolfgang, Tomko Robert J. Jr., and Sakata Eri. (2018) Expanded coverage of the 26S proteasome conformational landscape reveals mechanisms of peptidase gating, Cell Rep. 24, 1301–1315. [PubMed: 30067984]

39. Beckwith Robyn, Estrin Eric, Worden Evan J., and Martin Andreas. (2013) Reconstitution of the 26S proteasome reveals functional asymmetries in its AAA+ unfoldase, Nat. Struct. Mol. Biol 20, 1164–1172. [PubMed: 24013205]

40. Baytshtok Vladimir, Chen Jiejin, Glynn Steven E., Nager Andrew R., Grant Robert A., Baker Tania A., and Sauer Robert T. (2017) Covalently linked HslU hexamers support a probabilistic mechanism that links ATP hydrolysis to protein unfolding and translocation, J. Biol. Chem 292, 5695– 5704 [PubMed: 28223361]

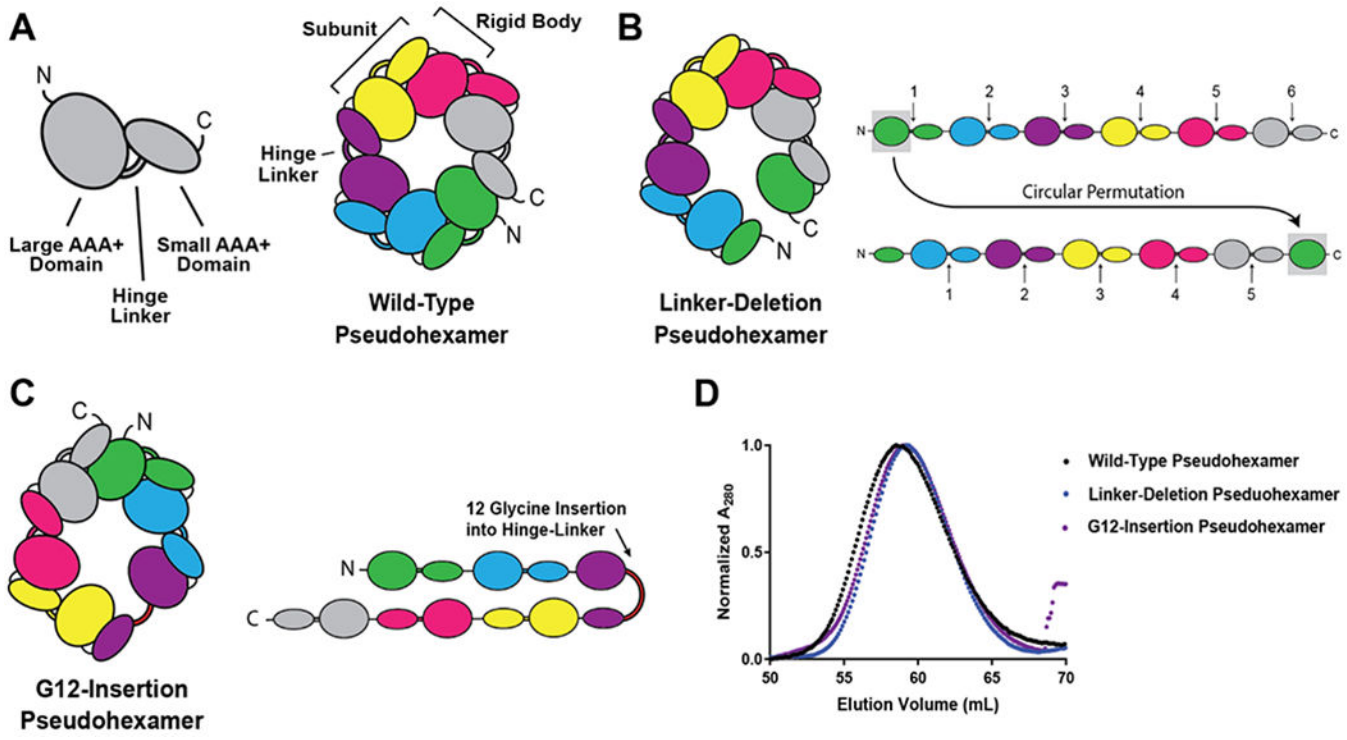


**Figure 1 –. Hinge-linker deletion and mutation in a single-chain ClpX$^{\Delta N}$ hexamer**

**(a)** Cartoon representation of a single subunit of ClpX$^{\Delta N}$ (left) and an assembled single-chain hexamer (right). **(b)** Cartoon representation of the linker-deletion pseudohexamer, which was constructed through circular permutation by moving the N-terminal large AAA+ domain of wild-type pseudohexamer to the C-terminus. **(c)** Cartoon representation of the G12-insertion pseudohexamer, which was constructed by adding 12 glycine residues into one hinge-linker of wild-type pseudohexamer. **(d)** Size exclusion chromatograms of single-chain pseudohexamer variants.

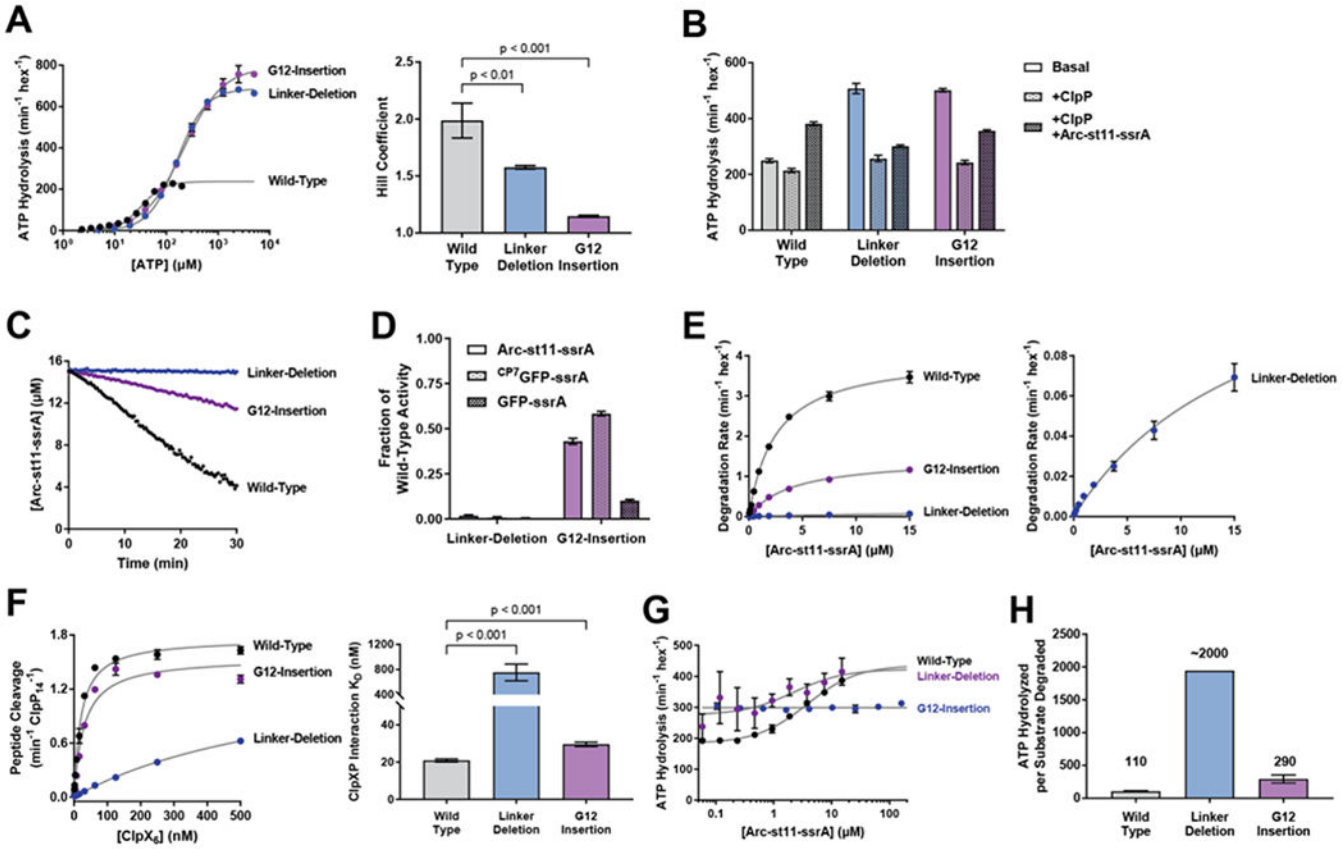


**Figure 2 –. Hinge-linker deletion and mutation impair intersubunit communication**

Unless noted, experimental values are averages of three independent replicates ± SD. Concentrations are given as follows: ClpX, pseudohexamer units; ClpP, 14-mer units; substrates, monomer units, **(a) Left** – Hill fits of the concentration dependence of ATP-hydrolysis rates. **Right** – Hill values with the significance of differences from wild type evaluated by a Student's two-tailed t-test for the hinge-linker deletion ($t = 4.6$, dof = 4, $p = 0.0098$) or G12 insertion ($t = 9.5$, dof = 4, $p = 0.0007$). **(b)** Rates of ATP hydrolysis by pseudohexamer variants alone (0.03 μM), in the presence of ClpP, or in the presence of ClpP and Arc-st11-ssrA. Linker-deletion pseudohexamer was tested at higher concentrations of ClpP and Arc-st11-ssrA because of its reduced affinity for both molecules (see panels **e** and **f**). Wild-type and G12-insertion pseudohexamers: 0.09 μM ClpP, 15 μM Arc-st11-ssrA. Linker-deletion pseudohexamer: 6.7 μM ClpP, 160 μM Arc-st11-ssrA. **(c)** Kinetics of degradation of fluorescent Arc-st11-ssrA (15 μM) by single-chain pseudohexamers (0.1 μM) and ClpP (0.3 μM). Data are representative of three replicates. **(d)** Degradation of Arc-st11-ssrA, $^{CP7}$GFP-ssrA, or GFP-ssrA (20 μM) by pseudohexamer variants (0.1 μM ClpX, 0.3 μM ClpP). Rates are plotted as a fraction of the wild-type rate, **(e) Left** – Michaelis-Menten plots of rates of Arc-st11-ssrA degradation by pseudohexamer variants (0.1 μM ClpX, 0.3 μM ClpP). **Right** – Same plot as left, rescaled to show fit of linker-deletion curve, **(f) Left** – pseudohexamer stimulation of ClpP (50 nM) cleavage of a fluorogenic peptide (15 μM). **Right** – $p$ values determined by Student's two-tailed t-test of $K_D$ differences between the wild type pseudohexamer and the hinge-linker deletion ($t = 9.6$, dof = 4, $p = 0.0006$) or G12

insertion ($t$= 11, dof = 4, $p$ = 0.0004). **(g)** Changes in ATP hydrolysis in response to increasing concentrations of Arc-st11-ssrA substrate. Wild-type and G12-insertion pseudohexamers: 0.1 μM ClpX, 0.3 μM ClpP, fit to an initial value and a hyperbolic increase to a saturated value. Linker-deletion pseudohexamer: 0.1 μM ClpX, 10 μM ClpP, fit to a constant linear value, **(h)** Energetic cost of ClpXP degradation of Arc-st11-ssrA supported by different pseudohexamers. Due to uncertainty inherent in the $V_{max}$ determined for linker-deletion pseudohexamer, the calculated energetic cost for this variant is approximate.

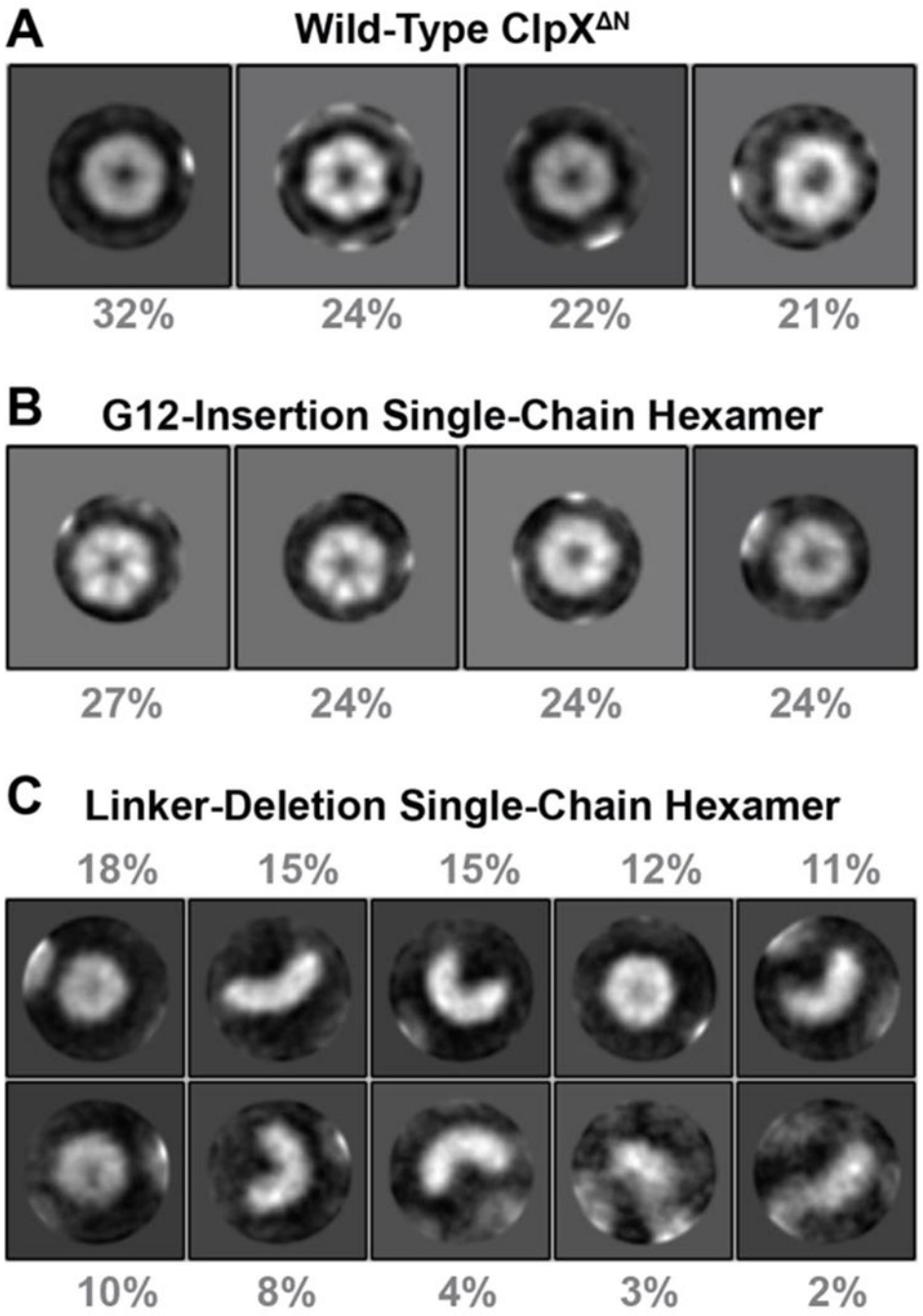


**Figure 3 –. Hinge-linker deletion disrupts ClpX ring structure**

2D class averages of negative-stain EM images of **(a)** wild-type ClpX$^{\Delta N}$ hexamers; **(b)** G12-insertion pseudohexamers; and **(c)** linker-deletion pseudohexamers. The percent of particles assigned to each class are indicated.

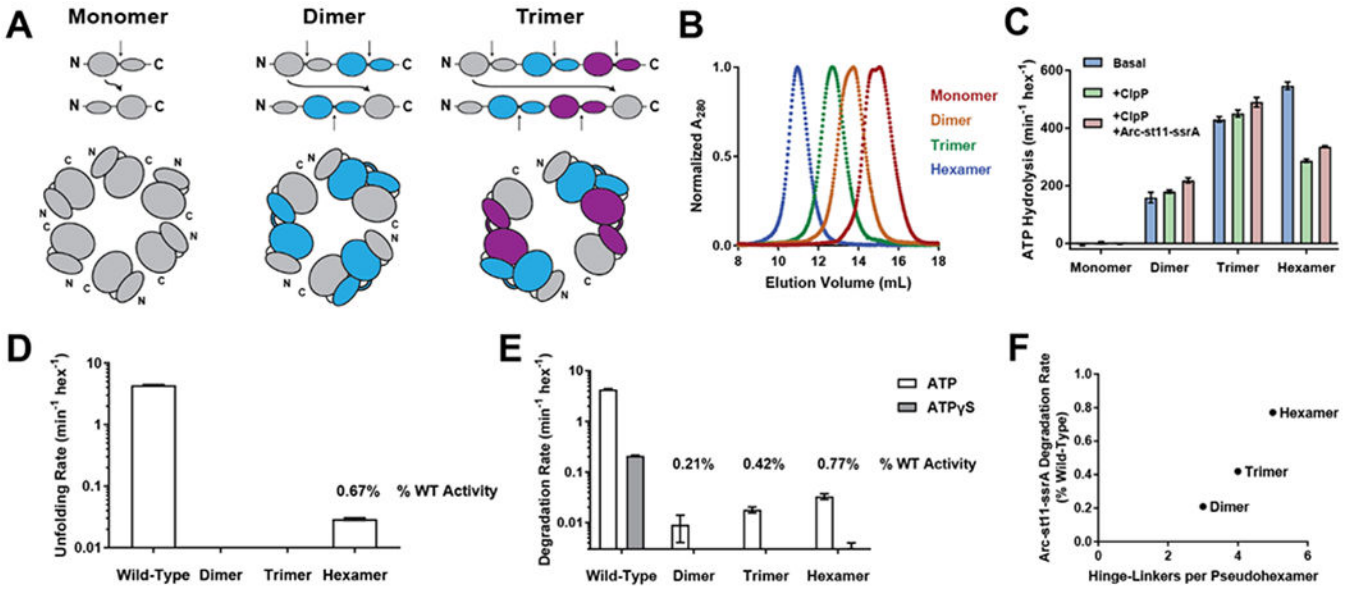


**Figure 4 –. Smaller hinge-linker variants fail to form hexamers**

Unless noted experimental values are averages of three independent replicates ± SD. Concentrations are given as follows: ClpX, pseudohexamer units; ClpP, 14-mer units; substrates, monomer units, **(a)** Construction of circularly permuted variants that delete hinge-linkers from ClpX$^{\Delta N}$ monomers, pseudodimers, and pseudotrimers. **(b)** Superdex 200 size-exclusion chromatography of linker-deletion variants, performed in the presence of 1 mM ADP, which stabilizes native ClpX$^{\Delta N}$ hexamers. **(c)** Rates of ATP hydrolysis by hinge-linker variants alone (0.1 μM), in the presence of ClpP (6.7 μM), or in the presence of ClpP (6.7 μM) and Arc-st11-ssrA (160 μM). **(d)** Rates of unfolding of Arc-Gcn4-ssrA (20 μM) by linker-deletion variants (0.3 μM) in the absence of ClpP plotted on a logscale. **(e)** Rates of degradation of Arc-st11-ssrA (15 μM) by linker-deletion variants (0.3 μM) in the presence of ClpP (0.9 μM) and ATP or ATPγS (10 mM) plotted on a logscale. **(f)** Arc-st11-ssrA degradation activity of linker-deletion variants (taken from panel **e**) plotted as a function of the number of hinge-linkers per hexamer equivalent.

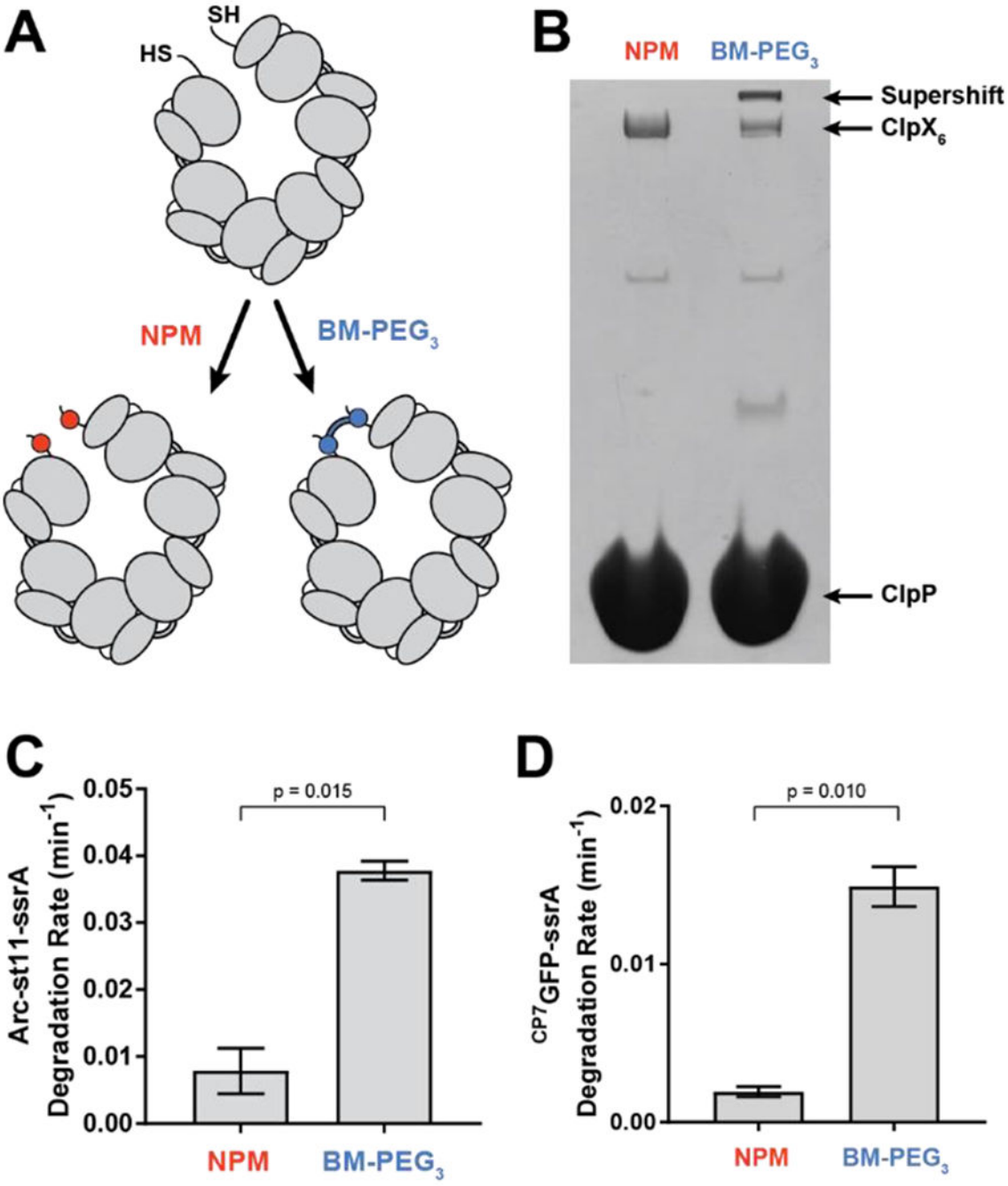


**Figure 5 –. Crosslinking a pseudohexamer with a hinge-linker deletion improves degradation**

**(a)** Cartoon of crosslinking and control reactions, **(b)** 10% SDS-PAGE analysis after the modification reactions depicted in panel A. The supershifted species corresponds to a circularized hexamer. Rates of Arc-st11-ssrA (20 μM monomer) **(c)** and $^{CP7}$GFP-ssrA (20 μM monomer) **(d)** degradation by the NPM- and BM-PEG$_3$-modified linker-deletion variants. Values are averages ± SEM of two independent sets of three replicates. Significance of differences determined by Student's two-tailed t-test are shown in panel C ($t$= 8.1, dof = 2) and panel D ($t$= 10, dof = 2).

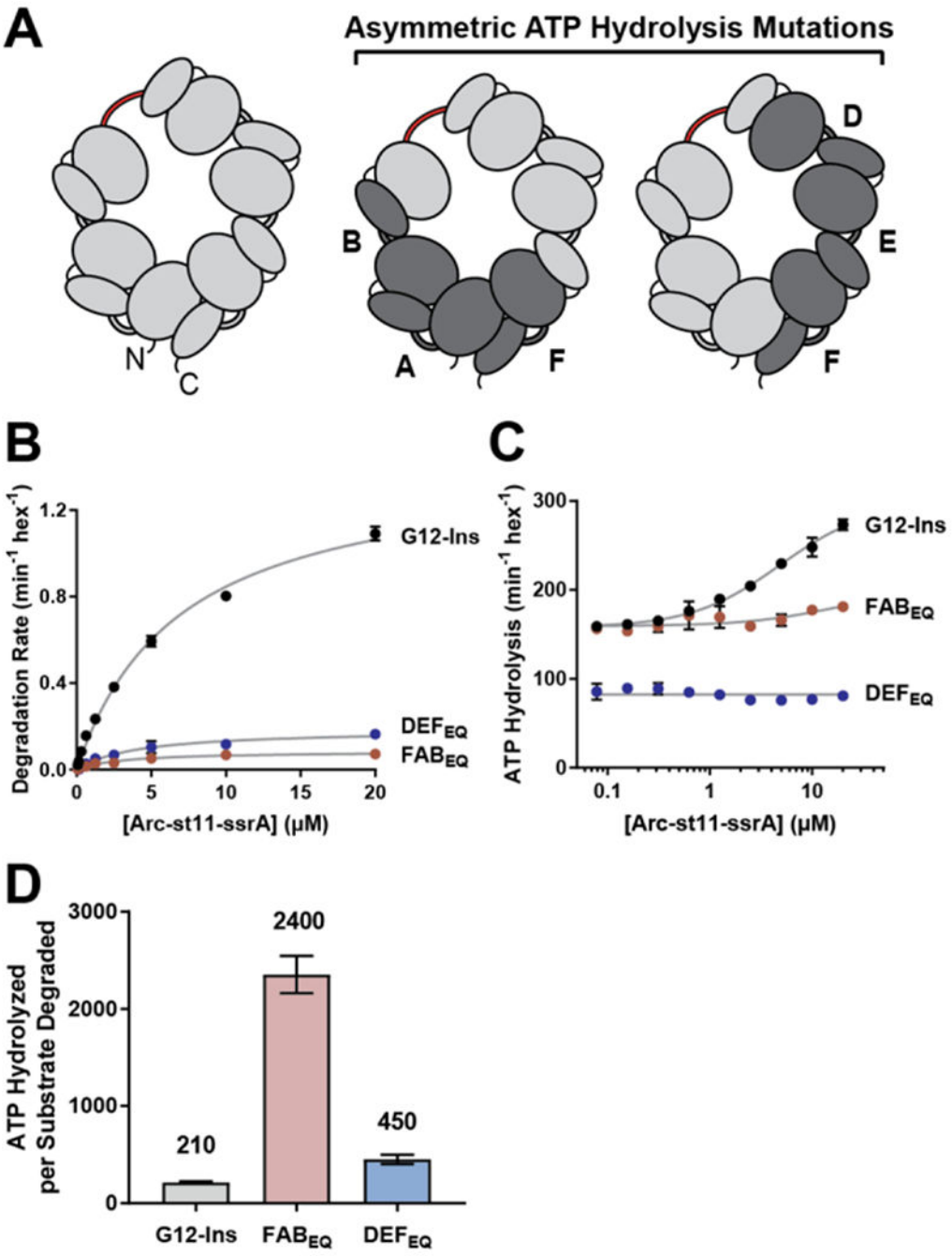


**Figure 6 –. Hinge-linker mutation reveals functional asymmetry**

Concentrations are given as follows: ClpX, pseudohexamer units; ClpP, 14-mer units; substrates, monomer units, **(a)** Cartoons of pseudohexamer variants with the substrate-binding face up. The G12 insertion is red; subunits with wild-type active-site residues for ATP hydrolysis are light gray; and subunits carrying the Walker-B E185Q ATP-hydrolysis mutation are dark gray, **(b)** Michaelis-Menten analysis of Arc-st11-ssrA degradation (0.1 μM pseudohexamer variants, 0.3 μM ClpP). Values are averages of three independent replicates ± SD. **(c)** Changes in ATP hydrolysis as a function of Arc-st11-ssrA concentration

were fit as described in the legend of panel 2G (0.1 μM pseudohexamer variants, 0.3 μM ClpP). Values are averages of three independent replicates ± SD. **(d)** Energetic cost of Arc-st11-ssrA degradation. Values are averages ± SEM of two independent sets of three replicates.

**Table 1 –**

**Fitted parameters from biochemical analysis of single-chain ClpX$^{\Delta N}$ hexamers**

Values are reported as average ± SD. The reported error was calculated by fitting independent replicates to curves, and then measuring the mean and variance of the resultant fitted parameters. Values labeled * are approximate because degradation rates for substrate concentrations above $K_M$ could not be tested.

| | | | |
|---|---|---|---|
| ***ATP hydrolysis* (Fig. 2A)** | | | |
| | **$V_{max}$ / $E_{TOT}$ ($min^{-1}$ $hex^{-1}$)** | **$K_M$ (μM)** | **n** |
| **Wild-Type** | 240 ± 10 | 33 ± 1 | 2.0 ±0.2 |
| **Linker-Deletion** | 670 ± 20 | 160 ± 10 | 1.6 ± 0.1 |
| **G12-Insertion** | 790 ± 30 | 220 ± 10 | 1.1 ±0.1 |
| | | | |
| ***Arc-st11-ssrA degradation* (Fig. 2E)** | | | |
| | **$V_{max}$ / $E_{TOT}$ ($min^{-1}$ $hex^{-1}$)** | **$K_M$ (μM)** | |
| **Wild-Type** | 4.1 ±0.2 | 2.5 ±0.2 | |
| **Linker-Deletion** | ~0.2 * | ~20 * | |
| **G12-Insertion** | 1.5 ± 0.1 | 4.1 ± 0.1 | |
| | | | |
| ***ClpP binding* (Fig. 2F)** | | | |
| | **$V_{max}$ / $E_{TOT}$ ($min^{-1}$ $Cl_PP_{14}^{-1}$)** | **$K_D$ (nM)** | |
| **Wild-Type** | 1.8 ± 0.1 | 21 ± 1 | |
| **Linker-Deletion** | 1.6 ± 0.1 | 750 ± 130 | |
| **G12-Insertion** | 1.6 ± 0.1 | 30 ± 1 | |
| | | | |
| ***ATP hydrolysis dependence on protein substrate concentration* (Fig.2G)** | | | |
| | **$V_{init}$ / $E_{TOT}$ ($min^{-1}$ $hex^{-1}$)** | **$V_{max}$ / $E_{TOT}$ ($min^{-1}$ $hex^{-1}$)** | **$K_{app}$ (μM)** |
| **Wild-Type** | 180 ± 10 | 440 ± 10 | 3.8 ± 0.8 |
| **Linker-Deletion** | - | 300 ± 10 | - |
| **G12-Insertion** | 190 ± 100 | 440 ± 90 | 2.2 ± 4 |
| | | | |
| ***Arc-st11-ssrA degradation* (Fig. 6B)** | | | |
| | **$V_{max}$ / $E_{TOT}$ ($min^{-1}$ $hex^{-1}$)** | **$K_M$ (μM)** | |
| **G12-Insertion** | 1.4 ± 0.1 | 6.9 ± 0.5 | |
| **G12-Ins, $FAB_{EQ}$** | 0.085 ± 0.006 | 3.0 ± 0.7 | |
| **G12-Ins, $DEF_{EQ}$** | 0.19 ± 0.02 | 4.5 ± 2 | |
| | | | |
| ***ATP Hydrolysis dependence on protein substrate concentration* (Fig. 6C)** | | | |
| | **$V_{init}$ / $E_{TOT}$ ($min^{-1}$ $hex^{-1}$)** | **$V_{max}$ / $E_{TOT}$ ($min^{-1}$ $hex^{-1}$)** | **$K_{app}$ (μM)** |
| **G12-Insertion** | 160 ± 10 | 300 ± 10 | 4.6 ± 0.4 |
| **G12-Ins, $FAB_{EQ}$** | 160 ± 10 | 200 ± 10 | 2.8 ± 4 |
| **G12-Ins, $DEF_{EQ}$** | - | 86 ± 1 | - |